Journal of Cellular Physiology

Increased Amyloid Precursor Protein and Tau Expression Manifests as Key Secondary Cell Death in Chronic Traumatic Brain Injury

SANDRA A. ACOSTA,[1] NAOKI TAJIRI,[1] PAUL R. SANBERG,[2] YUJI KANEKO,[1] AND CESAR V. BORLONGAN[1]*

[1]*Department of Neurosurgery and Brain Repair, Center of Excellence for Aging and Brain Repair, University of South Florida Morsani College of Medicine, Tampa, Florida*

[2]*Office of Research and Innovation, Department of Neurosurgery and Brain Repair, University of South Florida, Tampa, Florida*

In testing the hypothesis of Alzheimer's disease (AD)-like pathology in late stage traumatic brain injury (TBI), we evaluated AD pathological markers in late stage TBI model. Sprague–Dawley male rats were subjected to moderate controlled cortical impact (CCI) injury, and 6 months later euthanized and brain tissues harvested. Results from H&E staining revealed significant 33% and 10% reduction in the ipsilateral and contralateral hippocampal CA3 interneurons, increased MHCII-activated inflammatory cells in many gray matter (8–20-fold increase) and white matter (6–30-fold increased) regions of both the ipsilateral and contralateral hemispheres, decreased cell cycle regulating protein marker by 1.6- and 1-fold in the SVZ and a 2.3- and 1.5-fold reductions in the ipsilateral and contralateral dentate gyrus, diminution of immature neuronal marker by two- and onefold in both the ipsilateral and contralateral SVZ and dentate gyrus, and amplified amyloid precursor protein (APP) distribution volumes in white matter including corpus callosum, fornix, and internal capsule (4–38-fold increase), as well as in the cortical gray matter, such as the striatum hilus, SVZ, and dentate gyrus (6–40-fold increase) in TBI animals compared to controls (P's < 0.001). Surrogate AD-like phenotypic markers revealed a significant accumulation of phosphorylated tau (AT8) and oligomeric tau (T22) within the neuronal cell bodies in ipsilateral and contralateral cortex, and dentate gyrus relative to sham control, further supporting the rampant neurodegenerative pathology in TBI secondary cell death. These findings indicate that AD-like pathological features may prove to be valuable markers and therapeutic targets for late stage TBI.

J. Cell. Physiol. 232: 665–677, 2017. *Journal of Cellular Physiology* Published by Wiley Periodicals, Inc.

An estimated 1.7 million people, including military personnel and athletes, suffer from traumatic brain injury (TBI) annually, accounting for approximately 52,000 deaths a year in the United States (Fabrizio and Keltner, 2010; Faul et al., 2010). Epidemiological evidence implicates secondary injuries, with long lasting neuropathologies, as a risk factor in late stage TBI for the development of dementia and neurodegenerative diseases, such as Alzheimer's disease (AD) (Thurman et al., 1999; Faul et al., 2010; Wang et al., 2011, 2013; Tajiri et al., 2013; Gardner and Yaffe, 2015).

The secondary injury associated with TBI is becoming recognized as equally detrimental as the primary insult because of ensuing morbidity. Indeed, the evolving cell death after the initial impact in TBI accounts for various poorly understood mechanisms such as calcium influx, glutamate accumulation, abnormal amyloid precursor protein (APP) expression, oxidative stress, and neurotoxic inflammation (Povlishock and Cristman, 1995; Ghajar, 2000; Hortobágyi et al., 2007; Werner and Engelhard, 2007; Loane and Byrnes, 2010; Chauhan, 2014; Hong et al., 2014). These biochemical events occur throughout the brain and causes gray and white matter degeneration coupled with motor and cognitive impairments which are key pathological symptoms of TBI survivors (Borgens and Liu-Snyder, 2012; Acosta et al., 2013; Chauhan, 2014).

Although the impact of TBI has been speculated on neurodegenerative outcomes, in that moderate and severe TBI more than doubles the risk of developing dementia and AD-like symptoms later in life (Strittmatter and Roses, 1995; Gottlieb, 2000; Johnson et al., 2013), the pathological link between TBI and AD remains unclear and it represents a significant unmet clinical need. The detection of exacerbated inflammation, multifocal axonal swellings with accumulated APP and amyloid beta peptides accompany post-mortem brain tissues of stroke, TBI, multiple sclerosis, and AD patients (Blumbergs et al., 1994; Mannix and Whalen, 2012; Johnson et al., 2013), are hallmarks of the cognitive dysfunction seen in several neuropathologies including TBI, in late stage traumatic encephalopathy (CTE) and AD (Mannix and Whalen, 2012). Hence, investigating the propagation of AD-like neuropathology in late stage TBI, through region-specific development of secondary damage, warrants fundamental investigations in order to better understand the long lasting

Conflict of interest: The authors have declared no conflict of interest.

Contract grant sponsor: Department of Defense USA;
Contract grant number: W81XWH-11-1-0634.

*Correspondence to: Cesar V. Borlongan, Department of Neurosurgery and Brain Repair, Center of Excellence for Aging and Brain Repair, University of South Florida Morsani College of Medicine, 12901 Bruce B. Downs Blvd, Tampa, FL 3361.
E-mail: cborlong@health.usf.edu

Manuscript Received: 6 June 2016
Manuscript Accepted: 3 October 2016

Accepted manuscript online in Wiley Online Library (wileyonlinelibrary.com): 4 October 2016.
DOI: 10.1002/jcp.25629

detrimental consequences of brain injury. In an effort to gain insights into the implication of developing AD pathology in late stage TBI, the present in vivo study was designed to test the hypothesis that abnormal protein (APP) aggregations, a hallmark AD feature (Chen et al., 2003; Hortobágyi et al., 2007), predisposes neurodegeneration in both gray and white matter. Here, we provided evidence that neuronal cell loss, inflammation, decreased cell proliferation and impaired neurogenesis, occurred in discreet neurostructures exhibiting abnormal intra-neuronal APP expressions, indicating an extensive AD-like neuropathology in advanced TBI.

Materials and Methods

Subjects

All experiments were conducted in accordance with the National Institute of Health Guide and Use of Laboratory Animals and were approved by the Institutional Animal Care and Use Committee of the University of South Florida, Morsani College of Medicine. Rats were housed two per cage in a temperature- and humidity-controlled room that was maintained on 12/12-h light/dark cycles. They had free access to food and water. All necessary steps were performed to minimize animal pain and stress throughout the study. Two-month-old Sprague–Dawley male rats (Harlan Laboratories, Indianapolis, IN) served as subjects and either exposed to sham or TBI surgery. All studies were performed by personnel blinded to the treatment condition.

Surgical procedures

Two-month-old Sprague–Dawley rats (n = 20) were subjected to either TBI using a controlled cortical impactor (CCI) (n = 14) or sham control (no TBI) (n = 6) (Pittsburgh Precision Instruments, Inc., Pittsburgh, PA). Deep anesthesia was achieved using 1–2% isoflurane, and it was maintained using a gas mask. All animals were fixed in a stereotaxic frame (David Kopf Instruments, Tujunga, CA). After exposing the skull, coordinates of −0.2 mm anterior and +0.2 mm lateral to the midline were used to impact the brain at the fronto-parietal cortex with a velocity of 6.0 m/sec reaching a depth of 1.0 mm below the Dura matter layer and remained in that position for 150 msec. The impactor rod was angled 15° vertically to maintain a perpendicular position in reference to the tangential plane of the brain curvature at the impact surface. A linear variable displacement transducer (Macrosensors, Pennsauken, NJ), which was connected to the impactor, measured the velocity and duration to verify consistency. Sham control injury surgeries consisted of animals exposed to anesthesia, scalp incision, craniectomy, and suturing. An electric drill was used to perform the craniectomy of about 2.5 mm radius with coordinates calculated from the bregma at −0.2 anterior and +0.2 mm lateral right. An automated thermal blanket pad and a rectal thermometer allowed maintenance of body temperature within normal limits. All animals were closely monitored post-operatively with weight and health surveillance recording as per IACUC guidelines. Rats were kept hydrated at all times, and the analgesic ketoprofen was administered after TBI surgery and as needed thereafter. Pre and post TBI, rats were fed regular rodent diet (Harlan Laboratories).

Hematoxylin and eosin analysis

Under deep anesthesia, rats were sacrificed at 6 months after TBI surgery, and perfused through the ascending aorta with 200 ml of ice cold phosphate buffer saline (PBS), followed by 200 ml of 4% paraformaldehyde (PFA) in PBS. Brains were removed and post-fixed in the same fixative for 24 h followed by 30% sucrose in phosphate buffer (PB) for 1 week. Coronal sectioning was carried out at a thickness of 40 μm by cryostat. Hematoxylin and eosin (H&E) staining was performed to evaluate the core impact injury produced by the CCI model of TBI. H&E staining was done on every sixth coronal section spanning the dorsal hippocampus. As shown in our previous studies (Gottlieb, 2000; Glover et al., 2012), we also demonstrated here that the primary damage produced by the CCI TBI model was to the fronto-parietal cortex. In addition, neurons stained with H&E were also analyzed to reveal cell death in hippocampal CA3 area. Starting at coordinates AP-1.7 mm and ending AP-3.8 mm from bregma (Paxinos and Watson, 2005), coronal brain sections (40 μm) collected covering the whole dorsal hippocampus. A total number of six sections per rat were used. Cells presenting with nuclear and cytoplasmic staining (H&E) were manually counted in the CA3 neurons. CA3 cell counting spanned the whole CA3 area, starting from the end of hilar neurons to the beginning of curvature of the CA2 region in both the ipsilateral and contralateral side. Sections were examined with Nikon Eclipse 600 microscope at 20×. All data are represented as mean values of total # of cells with ± SEM.

Immunohistochemistry

Alternate brain sections were processed for immunohistochemistry. Staining for the cell cycle–regulating protein Ki67, DCX, APP, and MHCII (OX6) was done on every sixth coronal section throughout the entire striatum and dorsal and ventral hippocampus. Sixteen free-floating coronal sections (40 μm) were incubated in 0.3% hydrogen peroxide (H_2O_2) solution followed by 1-h of incubation in blocking solution (0.1 M phosphate-buffered saline (PBS) supplemented with 3% normal goat serum and 0.2% Triton X–100). Sections were then incubated overnight with rabbit anti rat Ki67 (1:400 cat# NCL-Ki67p; Nocastra), goat anti rat DCX (1:150 cat# sc-8066; Santa Cruz), rabbit anti rat APP (1:100 cat# A8717; Sigma), and mouse anti rat MHCII (1:750 cat# 554926; BD) antibody markers in PBS supplemented with 3% normal goat serum and 0.1% Triton X–100. Sections were then washed and biotinylated secondary antibody (1:200; Vector Laboratories, Burlingame, CA) in PBS supplemented with 3% normal goat serum, and 0.1% Triton X–100 was applied for 1 h. Next, the sections were incubated for 60 min in avidin–biotin substrate (ABC kit, Vector Laboratories). All sections were then incubated for 1 min in 3,30-diaminobenzidine (DAB) solution (Vector Laboratories). Sections were then mounted onto glass slides, dehydrated in ethanol and xylene, and cover-slipped using mounting medium. Of note, adequate positive and negative controls were performed to each antibody to confirm specificity.

Stereological analysis

Unbiased stereology was performed on brain sections immunostained with Ki67, DCX, APP, and MHCII. Sets of 1/6 section, about 240 μm apart, were taken from the brain spanning AP −0.2 mm to AP −3.8 mm in all 24 rats. Cell proliferation, differentiation into immature neurons, activated MHCII+ cells, neuronal APP were visualized by staining with Ki67, DCX, APP, and MHCII (OX6), respectively. Positive stains were analyzed with a Nikon Eclipse 600 microscope and quantified using Stereo Investigator software, version 10 (MicroBrightField, Colchester, VT). Ki67 (Scholzen and Gerdes, 2000), and DCX positive cells were counted within the subgranular zone (SGZ) and the subventricular zone (SVZ), in both hemispheres (ipsilateral and contralateral), using the optical fractionator probe of unbiased stereological cell counting technique. The estimated volume of APP and MHCII-positive cells was examined using the Cavalieri estimator probe of the unbiased stereological cell technique (Mayhew, 1991) revealing the volume of APP and MHCII in the cortex, striatum, hilus, thalamus, SVZ, dentate gyrus (DG), fornix, internal capsule, and corpus callosum in both hemispheres (ipsilateral and contralateral). The sampling was optimized to count at least 300 cells per animal with error coefficients less than 0.07. Each counting frame for optical fractionator (100 × 100 μm for Ki67, and DCX) was placed at an intersection of the lines

forming a virtual grid (125 × 125 μm), which was randomly generated and placed by the software within the outlined structure. The Cavalieri estimator is typically executed using a point grid spaced equally both across and down. The grid space used was of 100 μm in order to cover the entire region of interest (ROI) (Mayhew, 1991). Section thickness was measured in all counting sites.

Immunofluorescent staining

Phosphorylation of tau at Ser202/Thr205 and oligomeric tau stainings were carried out using the epitope AT8 and T22, respectively. Both tau species were conducted on every 1/3 sections, 40 μm thick, coronal brain sections. Coronal brain sections were washed three times for 10 min in 0.1 M TBS. Six sections were incubated with saline sodium citrate (SSC) solution at PH 6.0 for 40 min at 80°C for antigen retrieval. Then, samples were blocked for 60 min at room temperature with 8% normal goat serum (Invitrogen, CA) in 0.1 M TBS containing 0.1% Tween 20 (TBST) (Sigma, St. Louis, MO). Sections were then incubated overnight at 4°C with mouse monoclonal anti-AT8 (p-Ser202/Thr205; 1:100; MN1020 Thermo Scientific,Waltham, MA) or rabbit polyclonal anti-T22 (1:600; ABN454 millipore) with 10% normal goat serum. Then, the sections were washed five times for 10 min in 0.1 M TBST and soaked in 5% normal goat serum in 0.1 M TBST containing corresponding secondary antibodies, goat anti-mouse igG-Alexa 488 (green) (1:400; Invitrogen) or goat anti-rabbit IgG-Alexa 594 (red) (1:1500; Invitrogen) for 90 min. Finally, coronal sections were washed five times for 10 min in 0.1 M TBST and three times for 5 min in 0.1 M TBS, processed for 1:300 Hoechst 33258 (bisBenzimideH 33258 trihydrochloride, Sigma) for 30 min, washed in 0.1 M TBS, and cover-slipped with Fluoromount (Aqueous Mounting Medium; sigma F4680). Coronal sections were examined using a confocal microscope (Olympus, Shinjuku, Tokyo, Japan). Control studies included exclusion of primary antibody substituted with 5% normal goat serum in 0.1 M TBS. No immunoreactivity was observed in these controls.

Analysis of fluorescent staining

From all sections, approximately 4–6 images of 20× magnification were taken from each coronal section using confocal microscopy (Olympus) and analyzed with ImageJ (National Institutes of Health, Bethesda, MD). All photomicrographs were converted to gray scale. Background was selected from blank control images, and subsequently used to subtract the background from all images. The same threshold was used for all images. Thereafter, the staining intensity of each section was quantified as the average optical density readings of four randomly selected areas within that section. The final staining intensity of each group resulted as the average of each staining intensity per section.

Statistical analysis

For data analyses, contralateral and ipsilateral corresponding brain areas were used as raw data providing two sets of data per treatment condition (TBI vs. sham control), therefore one-way analysis of variance (ANOVA) was used for group comparisons, followed by subsequent pairwise comparisons; post hoc tests Bonferroni's test. All data are represented as mean values with ± SEM. Statistical significance was set at $P < 0.05$ for all analyses.

Results

Preliminary analyses of these data, comparisons between sham control ipsilateral and sham control contralateral side, throughout all brain areas analyzed, demonstrated not significant differences ($P > 0.05$). Thus, the data from both sides of the sham group were combined.

Decreased cell proliferation, impaired neurogenesis, and rampant hippocampal cell loss in late stage TBI

ANOVA revealed significant treatment effects on cell proliferation (Ki67+) in SVZ and DG ($F_{2,15} = 39.51$, $P < 0.0001$; $F_{2,15} = 45.35$, $P < 0.0001$), as well as on neurogenesis (DCX+) in SVZ and DG ($F_{2,15} = 17.60$, $P < 0.0001$; $F_{2,15} = 16.47$, $P < 0.0001$) (Fig. 1). Post hoc test revealed significant decrements in cell proliferation (Ki67+) in the ipsilateral SVZ and DG of TBI animals relative to the contralateral SVZ and DG respectively of TBI animals (P's < 0.001). Similarly, there were significant reductions in cell proliferation (Ki67+) in the ipsilateral (P's < 0.001), and the contralateral (P's < 0.05) SVZ and DG of TBI animals compared to sham animals. In addition, there were significant diminution of neurogenesis (DCX+) in the ipsilateral SVZ and DG of TBI animals compared to the contralateral SVZ and DG respectively of TBI animals (P's < 0.001). Likewise, there were significant decrements in neurogenesis (DCX+) in the ipsilateral SVZ and DG (P's < 0.001) of TBI animals compared to sham animals. DCX+ cells were significantly reduced on the contralateral (P's < 0.001) DG of TBI animals, but not the contralateral ($P > 0.05$) SVZ of TBI animals compared to sham animals. Furthermore, ANOVA revealed significant treatment effects on hippocampal CA3 cells loss ($F_{2,15} = 54.27$, $P < 0.0001$). Post hoc test revealed significant hippocampal CA3 cells loss in the ipsilateral side compared to the contralateral side of TBI animals ($P < 0.05$). There were 33% and 10% reduction of hippocampal CA3 cells in the ipsilateral and contralateral side, respectively of hippocampal CA3 interneurons of TBI animals compared to sham animals (P's < 0.001) (Fig. 1).

Region-specific exacerbation of MHCII+ activated cells in gray and white matter areas in late stage TBI

The estimated volume of MHCII+ activated cells was quantified using stereological techniques. ANOVA revealed overall significant treatment effect on inflammation in cortical and subcortical regions as evidenced by MHCII immunostaining in all gray matter regions examined here as follows: cortex ($F_{2,15} = 47.78$, $P < 0.0001$); striatum ($F_{2,15} = 40.54$, $P < 0.0001$); DG ($F_{2,15} = 43.16$, $P < 0.0001$); hilus ($F_{2,15} = 35.44$, $P < 0.0001$); SVZ ($F_{2,15} = 80.04$, $P < 0.0001$); and thalamus ($F_{2,15} = 6.484$, $P < 0.001$) (Fig. 2). Posthoc test revealed significant upregulations of activated MHCII+ cells in the ipsilateral side of TBI animals compared to their contralateral side across all gray matter areas analyzed (P's < 0.0001), except hilus and thalamus ($P > 0.05$). There were significant upregulations of activated MHCII+ cells in both ipsilateral and contralateral gray matter areas of TBI animals in all gray matter regions examined compared to sham animals (P's < 0.0001) (Fig. 2).

Similarly, ANOVA demonstrated significant treatment effects on inflammation in several white matter subcortical regions as evidenced by MHCII+ immunostaining in all regions examined here as follows: corpus callosum ($F_{2,15} = 786.2$, $P < 0.0001$); fornix ($F_{2,15} = 21.92$, $P < 0.0001$); and internal capsule ($F_{3,15} = 198.9$, $P < 0.0001$) (Fig. 3). Posthoc test revealed no significant difference of activated MHCII+ cells in the ipsilateral side of TBI animals compared to their contralateral side across all white matter areas analyzed (P's > 0.05). However, there were significant upregulations of activated MHCII+ cells in both ipsilateral and contralateral side of TBI animals across all white matter areas analyzed compared to sham animals (P's < 0.0001) (Fig. 3).

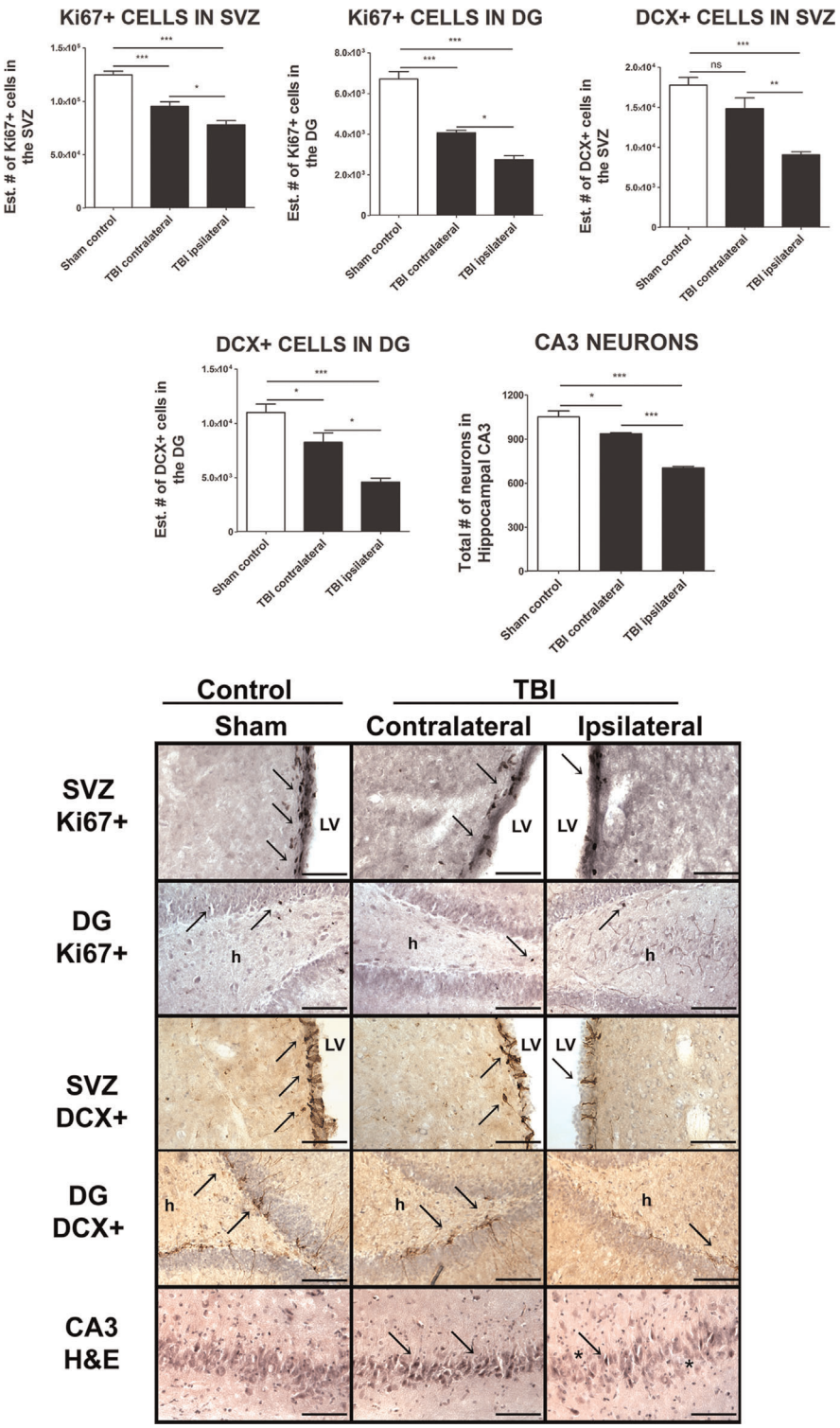

Fig. 1. Reduced cell proliferation, impaired neurogenesis, and increased hippocampal cell loss in late stage TBI. Part A, quantitative stereological analysis revealed significant decrements in cell proliferation and neurogenesis in the SVZ and DG after late stage TBI compared to sham animals ($^{*}P$'s < 0.05). Part A, bottom right, quantitative analyses of total number of CA3 neurons revealed a significant increase in neuronal cell loss after TBI compared to sham animals ($^{*}P$'s > 0.05). Part B, top, photomicrographs are representative coronal brain sections of the corresponding ipsilateral and contralateral side of the SVZ, and DG regions stained with a cell proliferation marker (Ki67), an immature neuronal marker (DCX) at 6 months post TBI of sham, and TBI animals. Arrows denote positive staining. Part B, bottom, photomicrographs are representative coronal brain sections staining with H&E from ipsilateral and contralateral CA3 area of the hippocampus of sham, and TBI animals. Arrows denote dark pink/purple cells characteristic of shrunken and condensed nuclei and hypereosinophilic cytoplasm, and neuronal cell loss within the CA3 region to the contralateral and ipsilateral side respectively in TBI animals. Scale bar: 50 μm. $^{*}P < 0.05$; $P < 0.05$, $^{**}P < 0.01$, $^{***}P < 0.001$. ns, not significant. Ki67 and DCX data are expressed as estimated # of positive cells. H&E data are expressed as total # of cells. Data are expressed as mean ± SEM.

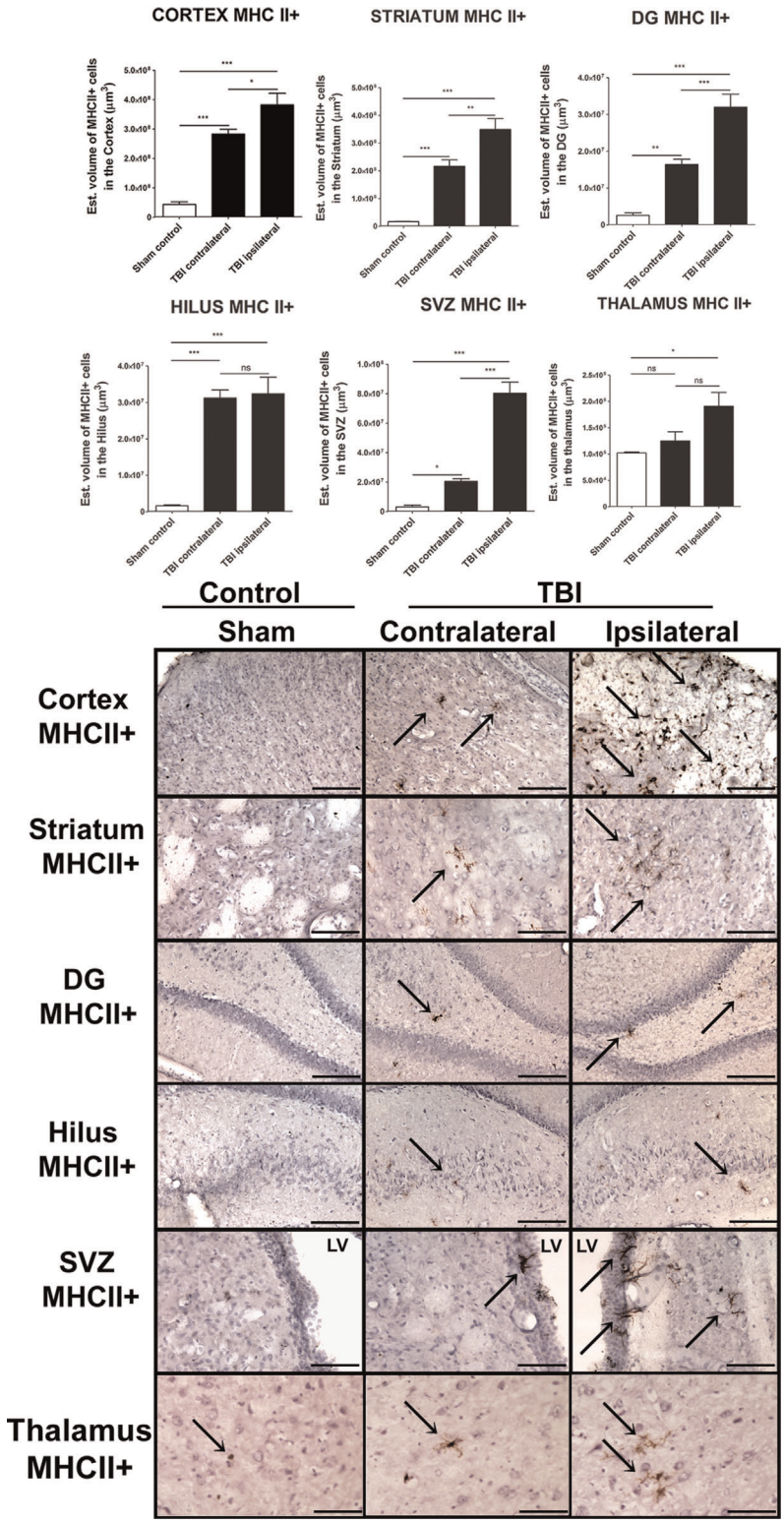

Fig. 2. Increased MHCII+ activated cells in proximal and remote gray matter areas in late stage TBI. Part A, stereological analysis of MHCII+ cells estimated volume in cortex, striatum, DG, and SVZ revealed significant upregulation of activated MHCII+ cells in the ipsilateral side of TBI animals compared to their contralateral side across all gray matter areas analyzed (P's < 0.0001), except hilus and thalamus ($P > 0.05$). There were significant upregulations of activated MHCII+ cells in both ipsilateral and contralateral gray matter areas of TBI animals (P's < 0.0001) compared to sham animals (P's < 0.05). Part B, photomicrographs are representative coronal brain sections showing gray matter areas ipsilateral to injury stained with M1 activated immune cells marker (MHCII) 6 months post TBI injury. Arrows indicate positive staining for activated MHCII+ cells in cortex, striatum, DG, hilus, SVZ, and thalamus. Scale bar = 50 μm. $^{*}P < 0.05$, $^{**}P < 0.01$, $^{***}P < 0.001$; ns, not significant. MHCII data are expressed as estimated volume of positive cells. Data are expressed as mean ± SEM.

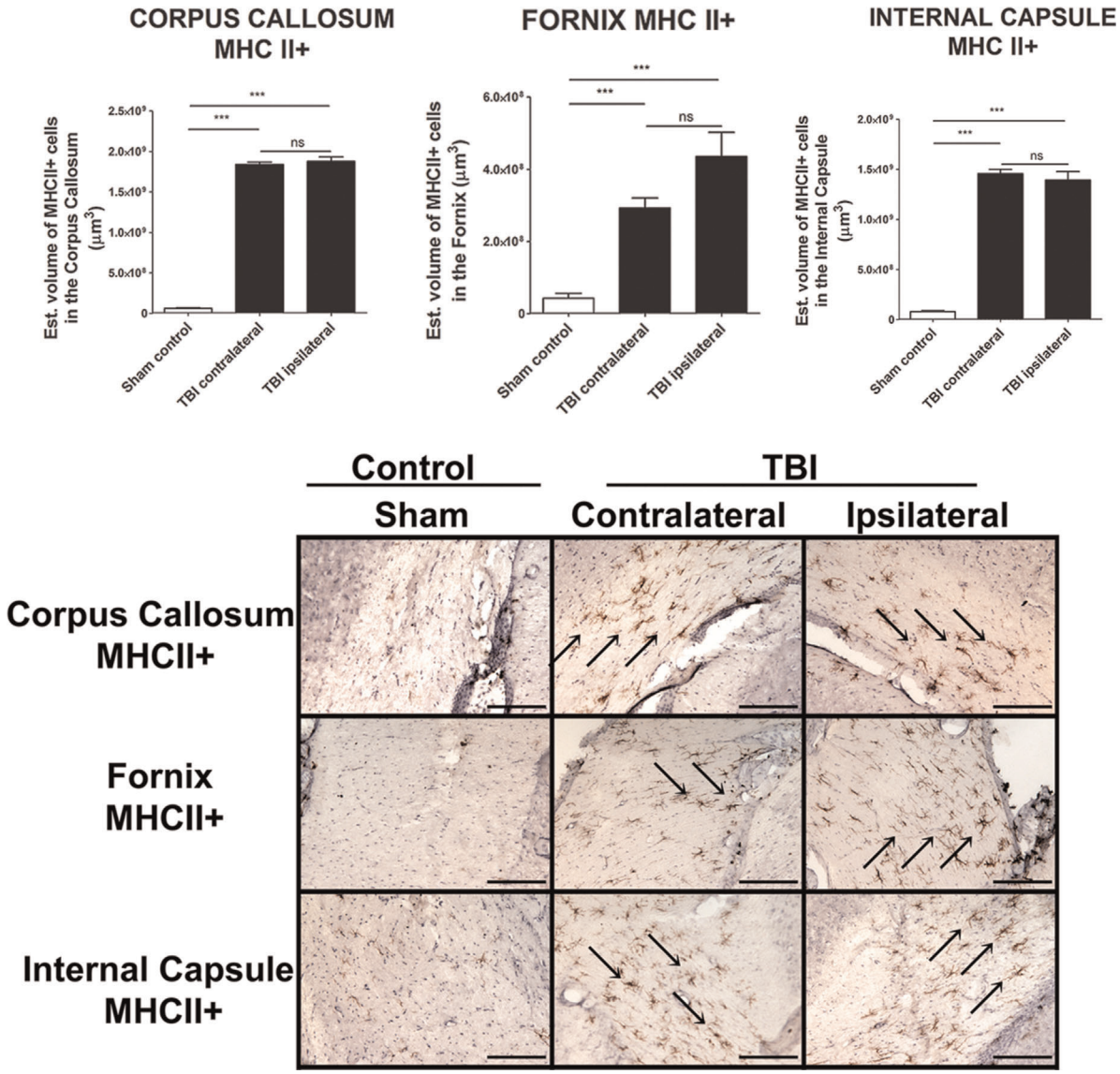

Fig. 3. Increased MHCII+ activated cells in proximal and remote white matter areas in late stage TBI. Part A, stereological analysis of MHCII+ cells estimated volume in corpus callosum, fornix, and internal capsule revealed no significant differences of activated MHCII+ cells in the ipsilateral side of TBI animals compared to their contralateral side across all white matter areas analyzed (P's > 0.05). There were significant upregulation of activated MHCII+ cells in both ipsilateral and contralateral side of TBI animals (P's < 0.0001) across all white matter areas analyzed compared to sham animals (P's < 0.05). Part B, photomicrographs are representative coronal brain sections showing white matter areas ipsilateral to injury stained with M1 activated immune cells marker (MHCII) 6 months post TBI injury. Arrows indicate positive staining for activated MHCII+ cells in corpus callosum, fornix, and internal capsule. Scale bar = 50 μm. $^{*}P < 0.05$, $^{**}P < 0.01$, $^{***}P < 0.001$; ns, not significant. MHCII data are expressed as estimated volume of positive cells. Data are expressed as mean ± SEM. Scale bar = 50 μm. $^{*}P < 0.05$, $^{**}P < 0.01$, $^{***}P < 0.001$; ns, not significant. Data are expressed as mean ± SEM.

Overexpression of APP+ cells in gray and white matter areas in late stage TBI

The estimated volume of APP+ expression was quantified using stereological techniques. The whole brain was examined to reveal TBI-induced APP+ overexpression in both gray and white matter areas (Fig. 4). ANOVA revealed overall significant treatment effect on APP+ in cortical and subcortical regions as evidenced by APP+ immunostaining in all gray matter regions examined here as follows: cortex ($F_{2,15} = 31.47$, $P < 0.0001$); striatum ($F_{2,15} = 256.3$, $P < 0.0001$); DG ($F_{2,15} = 21.37$, $P < 0.0001$); hilus ($F_{2,15} = 18.68$, $P < 0.0001$); and SVZ ($F_{2,15} = 4.435$, $P < 0.05$), except thalamus ($F_{2,15} = 0.222$, $P > 0.05$). Posthoc test revealed significant overexpression of APP+ cells in the ipsilateral side of TBI animals compared to their contralateral side across all gray matter areas analyzed (P's < 0.0001), except SVZ ($P > 0.05$). There were significant overexpressions of APP+ cells in both ipsilateral and contralateral in all gray matter areas analyzed of TBI animals compared to sham animals (P's < 0.0001) (Fig. 4).

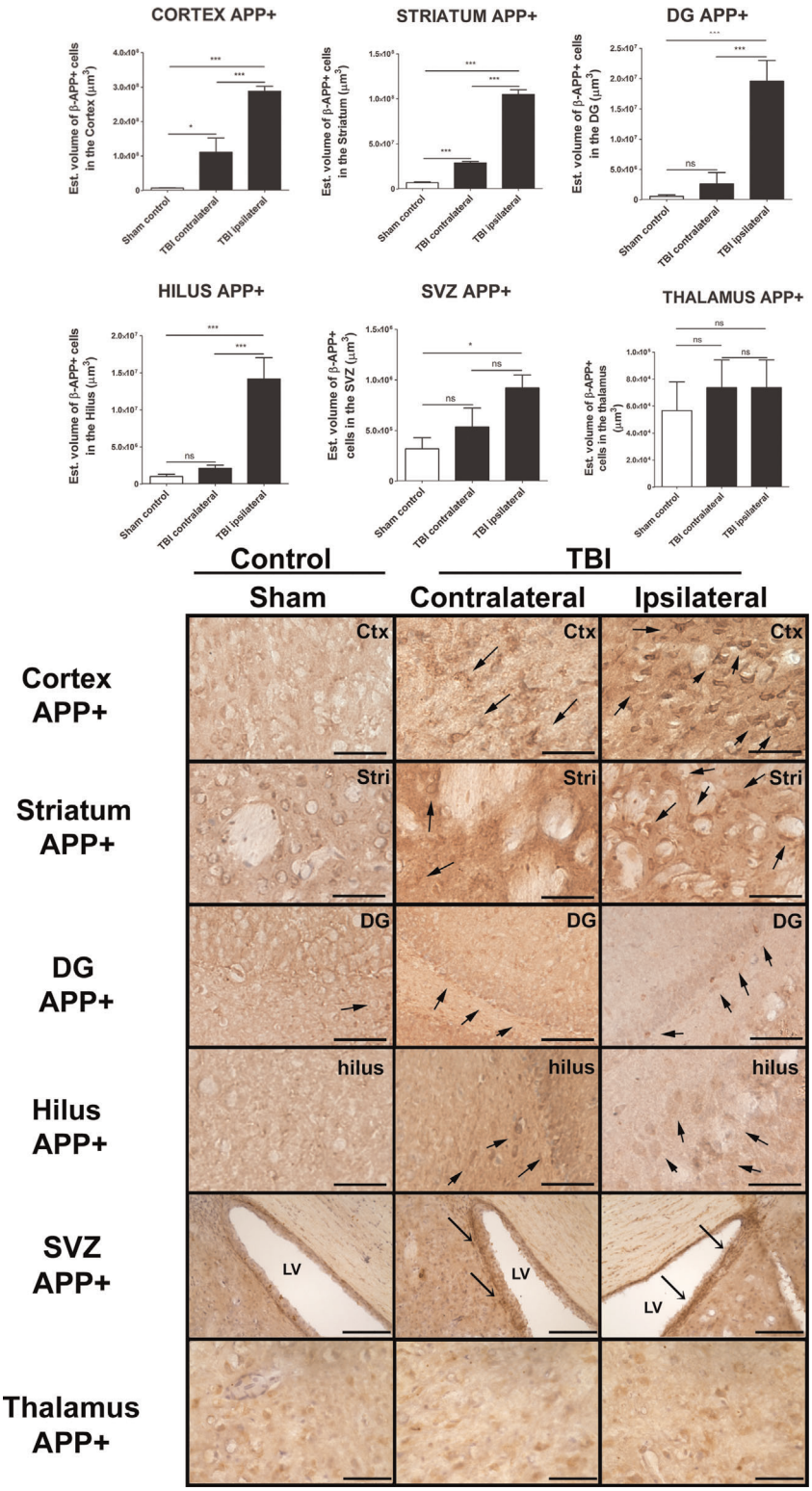

Fig. 4. Overexpression of intra-neuronal APP in proximal and remote gray matter areas in late stage TBI. Part A, stereological analysis of APP+ neurons estimated volume in cortex, striatum, DG, and hilus revealed significant increase of APP+ neurons in the ipsilateral side of TBI animals compared to their contralateral side across all gray matter areas analyzed (P's < 0.0001), except SVZ and thalamus ($P > 0.05$). There was significant overexpression of APP+ expressing neurons in both ipsilateral and contralateral gray matter areas of TBI animals (P's < 0.0001) compared to sham animals (P's < 0.05), except DG, hilus, SVZ, and thalamus (P's > 0.05). Part B, photomicrographs are representative coronal brain sections showing gray matter areas ipsilateral to injury stained with APP marker post TBI injury. Arrows indicate overexpression of intra-neuronal APP staining in cortex, striatum, DG, hilus, and SVZ. Scale bar = 50 μm. $^{*}P < 0.05$, $^{**}P < 0.01$, $^{***}P < 0.001$; ns, not significant. APP data are expressed as estimated volume of positive cells. Data are expressed as mean ± SEM.

Similarly, ANOVA demonstrated significant treatment effects on overexpression of APP in white matter subcortical regions as evidenced by APP+ immunostaining in all regions examined here as follows: corpus callosum ($F_{2,15} = 297.34$, $P < 0.0001$); fornix ($F_{2,15} = 121.4$, $P < 0.0001$); and internal capsule ($F_{2,15} = 190.2$, $P < 0.0001$) (Fig. 5). Posthoc test revealed significant overexpressions of APP+ cells in the ipsilateral side of TBI animals compared to their contralateral side across all white matter areas analyzed (P's < 0.0001). There were significant overexpressions of APP+ cells in both ipsilateral and contralateral white matter areas of TBI animals compared to sham animals (P's < 0.0001) (Fig. 5).

Increased expression of phosphorylated tau (AT8) in the cortex and in the dentate gyrus of the hippocampus in late TBI

The expression of phosphorylated tau, AT8+ cells, was quantified using immunofluorescent techniques and analyzed with Image J software. ANOVA revealed significant treatment effect on phosphorylated tau as evidenced by AT8+

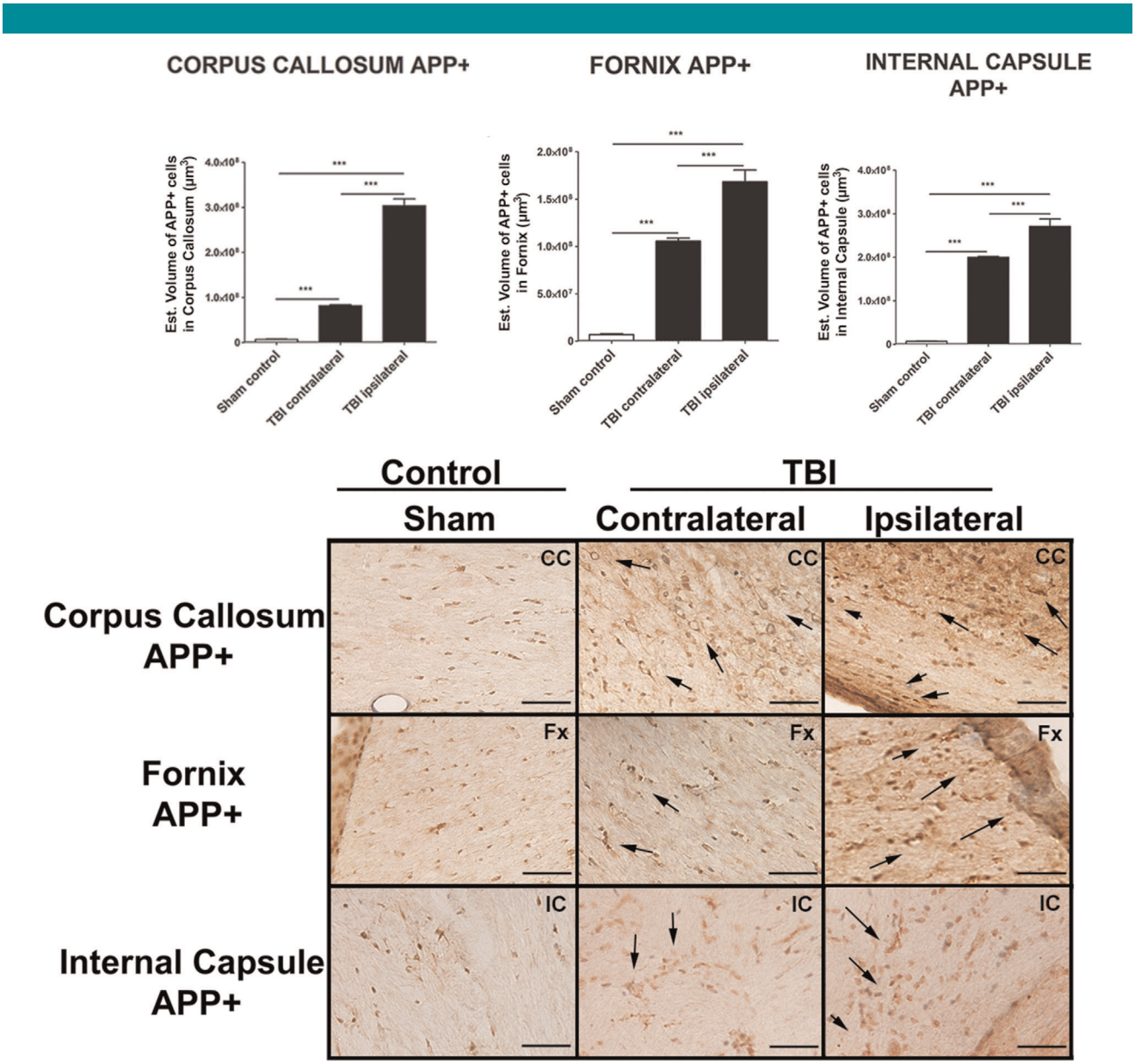

Fig. 5. Overexpression of APP in proximal and remote white matter areas in late stage TBI. Part A, stereological analysis of APP estimated volume in corpus callosum, fornix, and internal capsule revealed significant overexpression of APP+ staining in the white matter ipsilateral side of TBI animals compared to their contralateral side across all areas analyzed (P's < 0.0001). There was significant overexpression of APP+ staining in both ipsilateral and contralateral white matter areas of all TBI animals (P's < 0.0001) compared to sham animals (P's < 0.0001). Part B, photomicrographs are representative coronal brain sections showing white matter areas proximal and remote from TBI injury and ipsilateral to injury stained with APP marker post TBI injury. Arrows indicate overexpression of APP staining in corpus callosum, fornix, and internal capsule. Scale bar = 50 µm. $^{*}P < 0.05$, $^{**}P < 0.01$, $^{***}P < 0.001$; ns, not significant. APP data are expressed as estimated volume of positive cells. Data are expressed as mean ± SEM.

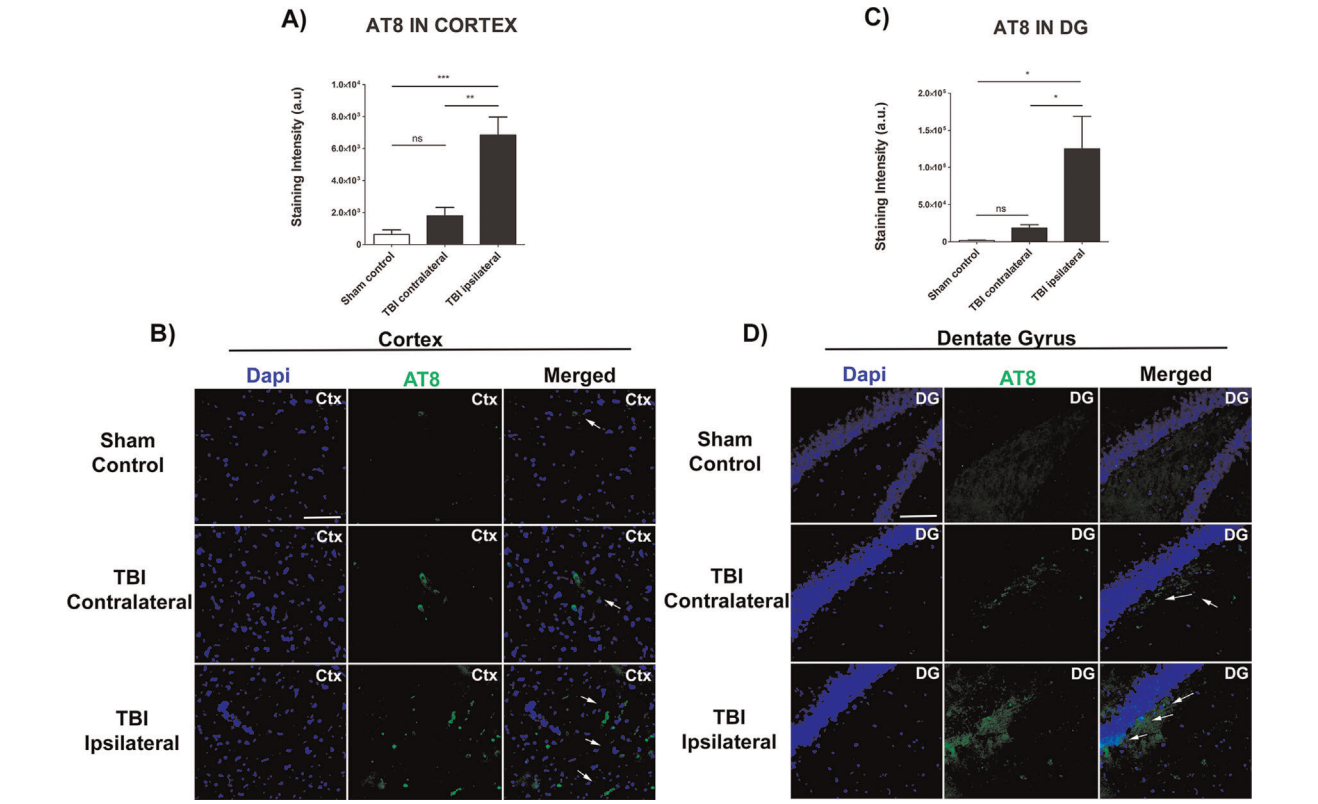

Fig. 6. TBI-induced tau phosphorylation at Ser202/Thr205 (AT8) in the cortex and dentate gyrus (DG) of the hippocampus 6 months post TBI. Part A and C, quantitative analysis of phosphorylated tau (AT8) expression in the cortex and DG revealed significant increase of phosphorylated tau in the ipsilateral and contralateral side of TBI animals compared to sham animals (*P*'s < 0.0001). Part B and D, confocal immunofluorescent images of phosphorylated tau (AT8) (green) and DAPI (blue) show positive expression in cortex and DG of late TBI injury. Arrows indicate positive expression of phosphorylated tau in the cell body of cortical and granular neurons. Scale bar = 50 μm. *P < 0.05, **P < 0.01, ***P < 0.001; ns, not significant. Phosphorylated tau (AT8) data are expressed as estimated staining intensity from positive cells. Data are expressed as mean ± SEM.

immunofluorescent staining in the frontal cortex ($F_{2,15} = 17.35$, $P < 0.0001$) and DG ($F_{2,15} = 6.895$, $P < 0.05$) (Fig. 6). Posthoc test revealed significant increased expression of AT8+ staining in the soma of ipsilateral cortex of TBI animals compared to their contralateral cortex ($P < 0.0001$). There were significant upregulations of AT8+ staining within neurons of both ipsilateral and contralateral cortex of TBI animals compared to sham animals (*P*'s < 0.05) (Fig. 6).

Evidence of oligomeric tau (T22) accumulation in the cortex and in the dentate gyrus of the hippocampus in late TBI

The expression of oligomeric tau, T22+ cells was quantified using immunofluorescent techniques and analyzed with Image J software. ANOVA revealed significant treatment effect on oligomeric tau as evidenced by T22+ immunofluorescent staining in the frontal cortex ($F_{2,15} = 8.933$, $P < 0.05$) and DG ($F_{2,15} = 23.43$, $P < 0.001$) of TBI animals (Fig. 7). Posthoc test revealed evidence of significant accumulation of T22+ tau species within the cytosol of cortical neurons and granular neurons in the DG of ipsilateral cortex of TBI animals compared to their contralateral cortex ($P < 0.05$). There were significant accumulation of T22+ tau within neurons of both ipsilateral and contralateral cortex of TBI animals compared to sham animals (*P*'s < 0.001) (Fig. 7).

Discussion

The present study demonstrated the propagation of secondary injury in brain regions proximal and remote to the primary core impact of injury in late stage TBI, characterized by AD-like pathology. That a neurogenerative process involving aberrant APP+, AT8, and T22 accumulations, reminiscent of AD, plagues TBI suggests overlapping cell death mechanisms between acute and late stage brain disorders. This progression of APP overexpression in advanced TBI was accompanied by a persistent cell loss in hippocampal CA3 neurons, reduced number of proliferating precursor cells and immature neurons, in neurogenic niches (i.e., SVZ and DG), and closely associated with exacerbation of MHCII inflammatory cells in specific brain regions displaying APP+ overexpression. The significant accumulations of additional AD-like phenotypic markers including amyloid precursor protein (APP) and tau (phosphorylated tau AT8 and oligomeric tau T22) in ipsilateral and contralateral cortex, and dentate gyrus relative to sham control further support the neurodegenerative feature of the secondary cell death in TBI.

The rationale for measuring Ki67+ cells was to determine the influence of late stage secondary injuries on the overall proliferative capacity of cells within specific regions regardless of fate of differentiation. Further image analysis of the location of the positive KI67 cells did not correlate with the location of

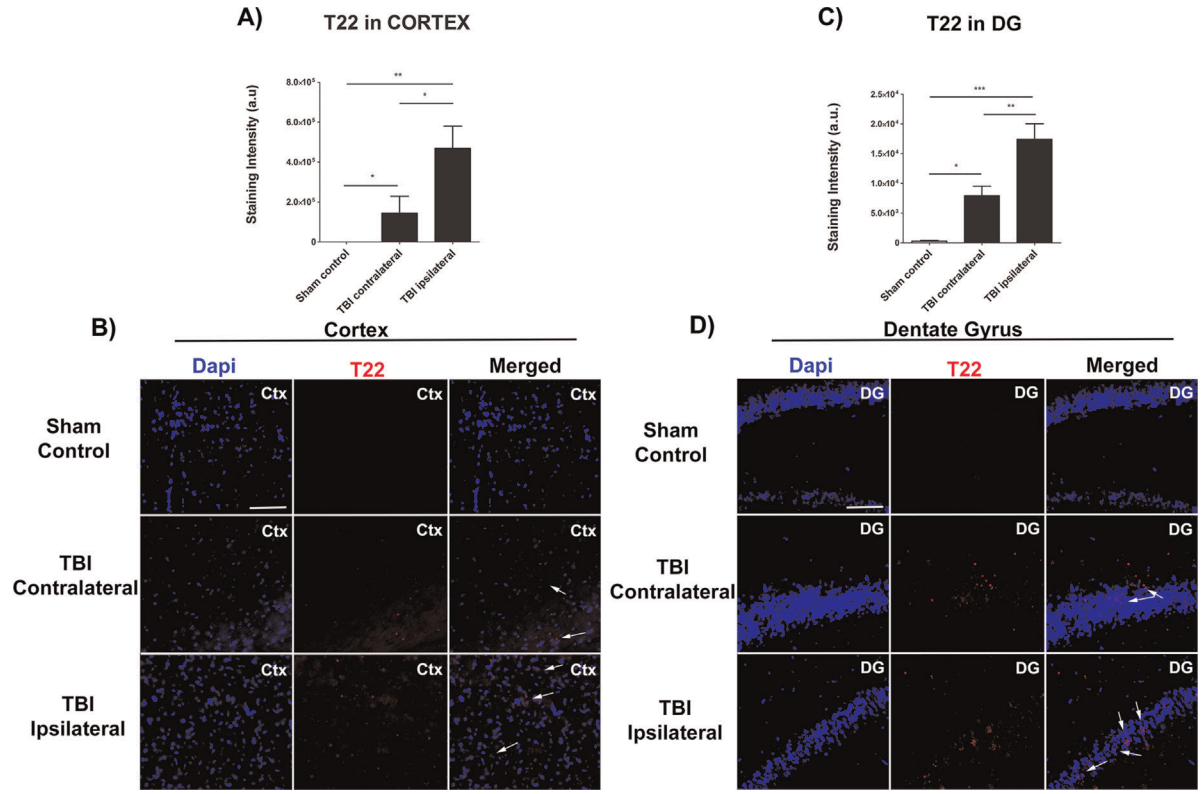

Fig. 7. TBI-induce accumulation of oligomeric tau (T22) in the cortex and dentate gyrus (DG) of the hippocampus 6 months post TBI. Part A and C, quantitative analysis of oligomeric tau (T22) accumulation in the cortex and DG revealed significant increase of in the ipsilateral and contralateral side of TBI animals compared to sham animals (*P*'s < 0.0001). Part B and D, confocal immunofluorescent images of oligomeric tau (T22) (red) and DAPI (blue) show positive expression in throughout cortex and in the soma of neurons from the DG. Arrows indicate positive expression of aggregates of oligomeric tau in the cortex and granular neurons in the DG. Scale bar = 50 μm. $^{*}P < 0.05$, $^{**}P < 0.01$, $^{***}P < 0.001$; ns, not significant. Oligomeric tau (T22) data are expressed as estimated staining intensity from positive cells. Data are expressed as mean ± SEM.

the MHCII+ cells, thus we discarded the possibility that MHCII+ cells were proliferating specifically at the neurogenic niches. Since the analysis showed a decreased on cell proliferation, then the next question was whether secondary injury also altered neurogenic capacity of the neurogenic niches. This required lineage specific characterization, which we pursued in this study using DCX as a marker of immature neurons. Clearly, additional lineage markers will be needed to fully assess the cell fate, but this will require a large study that is best addressed in the future. Collectively, these observations support our hypothesis that neurodegeneration in TBI progresses via an AD pathological mechanism involving APP+ overexpression.

The onset of cognitive deficits has been documented in TBI patients presenting with AD-like pathology (Fleminger et al., 2003; Vasterling et al., 2012; Aungst et al., 2014; Sharp et al., 2014). The detection of increased APP+ expression, in tandem with impaired neurogenesis, in the hippocampus may lead to dysfunctions in hippocampal-mediated cognitive performance (Reddy et al., 2010; Zhao et al., 2011). Of note, robust hippocampal plasticity likely participates in learning and memory consolidation, a crucial process in cognitive function (Scoville, 1954; Amaral and Witter, 1989; Nakashiba et al., 2008). That such hippocampal neurodegeneration, seen to underlie many of cognitive impairments of AD, similarly manifests in TBI may explain the evolution of learning and memory deficits in TBI. Indeed, cognitively impaired experimental TBI animals present with APP+ deposition with coincident apoptosis and reduced neurogenesis in the hippocampus (Murakami et al., 1998; Kempermann, 2002; Rola et al., 2006; Park et al., 2014). To date, these published reports document the progressive amyloidosis in acute and subacute TBI; the present findings of APP+ in late stage TBI support the notion that AD hippocampal neurodegeneration, including likely the accompanying cognitive impairment, is not transient, but permanent sequelae of the TBI event (Strittmatter and Roses, 1995; Gottlieb, 2000; Hernandez-Ontiveros et al., 2013; Soldatovic-Stajic et al., 2014; Lozano et al., 2015).

We previously characterized chronic neuroinflammation in brain regions remote from the primary impacted area at 2 months after TBI (Acosta et al., 2013). Although some studies have reported that MHCII is not a specific marker for Th1/M1 pro-inflammatory cells, in that MHCII is also expressed in some M2 anti-inflammatory cells, our study used a clone of OX-6 which is exclusively expressed as an MHCII antigen when immune cells are fully activated during inflammatory responses (McLaurin et al., 1995; Marshall et al., 2013). Comparing our previous study (Acosta et al., 2013) and the present one based on MHCII analyses revealed that at 2 months post-TBI significant exacerbation of OX-6 positive activated MHCII cells were relegated to regions ipsilateral to injury including gray and white matter regions, whereas at 6 months post-TBI, there was a clear exacerbated inflammatory pathology characterized by increased OX-6 positive activated MCHII cells in the ipsilateral

area that trespassed into the contralateral side including anterior-proximal and remote-posterior to the original injury. Moreover, in the 2 months post-TBI model we demonstrated significant downregulation of Ki67-positive proliferating cells in ipsilateral SVZ and ipsilateral SGZ relative to sham control. Analysis of neurogenic niches, after 2 months post-TBI, revealed that only trends of reduced neurogenesis (DCX-positive immature neuronal cells) in ipsilateral SVZ and ipsilateral SGZ were detected relative to contralateral and sham control. However, in the 6 months post-TBI model, Ki67-positive proliferating cells were downregulated in both ipsilateral and contralateral SVZ and SGZ relative to sham control. In addition, there was a significant diminution of neurogenesis in both the ipsilateral and contralateral SVZ and SGZ relative to sham controls. After 2 months post-TBI, results from H&E staining demonstrated a significant decrease of hippocampal pyramidal neurons in the CA3 region ipsilateral to injury compared to sham control. There was no cell loss found in the contralateral side in the CA3 region at this 2-month TBI time point. In contrast, after 6 months post-TBI, a significant 33% and 10% cell loss was found in both the ipsilateral and contralateral side, respectively in the CA3 of the hippocampus. It is important to highlight that in the present 6 months post-TBI period, delayed secondary injury maintained a significant MHCII cells recruitment and activation in the ipsilateral hemisphere and such inflammatory response could now be seen trespassing or invading the contralateral side. Finally, laboratory evidence from acute and long-term studies suggests that many of the TBI models can lead to progressive pathological changes reflected in both brain and behavior, characterized by worsening cortical cell loss, tissue atrophy, and impaired neurotransmission coupled with cognitive decline, which were more pronounced in the chronic stage of injury (Dixon et al., 1999).

Prolonged exacerbation of activated MHCII+ cells were detected in gray matter structures such as cortex, striatum, thalamus, and white matter including corpus callosum, fornix, and cerebral peduncles. These findings support clinical observations demonstrating secondary progressive injury to both gray and white matter areas associated with long-term cognitive impairments in TBI patients (Schmidt et al., 2005; Rogers and Read, 2007; Ramlackhansingh et al., 2011; Elder, 2012). Specifically, at 2 months after TBI, the areas with the largest volume of activated MHCII+ cells were found in the cortex and the thalamus. These findings correlate with pre-clinical and clinical evidence that demonstrate that cerebral blood flow to cortex and thalamus is significantly abrogated even by mild TBI and coincides with cortical and thalamic atrophy which instigate impairments in executive function, speech, and in learning and memory (Ge et al., 2009; Little et al., 2010).

In the present in vivo study, we examined the progressive neuroinflammation at a much more late stage of TBI (i.e., 6 months). Interestingly, here, the thalamus did not show evidence of exacerbated inflammatory activation or increase APP overexpression, which may indicate spontaneous recovery of this specific brain region at the very late stage of TBI. Hemodynamic and cerebrovascular impairments are associated with chronic secondary injury after TBI (Hayward et al., 2011). Indeed, a significant decrease in cerebral blood flow (CBF) accompanies vascular damage in cortex, hippocampus and thalamus, and coincides with caspase overexpression, APP accumulation, exacerbated MHCII activation, and cell death during acute, subacute, and chronic time points after TBI (Scholzen and Gerdes, 2000; Hayward et al., 2010, 2011; Schiff, 2010). A recent study revealed long-term functional recovery and its association with vascular remodeling in the thalamus at later chronic stage (i.e., 8 months) in a TBI model (Hayward et al., 2011). Structural MRI and CBF measurements showed 13–56% reductions in CBF in the perilesional cortex and hippocampus. In contrast, the ipsilateral thalamus exhibited a 34% increment in CBF that correlated with a remarkable increase in blood vessel density. However, regardless of the enhanced CBF and vessel structure, animals did not show improvement in motor functions (Hayward et al., 2010). The present results showed that progressive neurodegeneration in TBI may present with region-specific AD-like pathologies amenable to neurovascular remodeling even at the late stage of the disease (Gottlieb, 2000; Schiff, 2010; Hayward et al., 2011). In-depth investigations into long-term brain remodeling may reveal discreet inflammatory processes within the neurovascular unit, allowing a better understanding of TBI pathology and its treatment.

Gray and white matter degeneration in the present study manifested as increased volume of activated MHCII+ neuroinflammatory cells detected within and adjacent to areas exhibiting APP+ overexpression in proximal and distal areas from the mechanical injury. This localized neuroinflammation and APP+ overexpression following TBI remains a poorly understood cell death mechanism. The present study focused on characterizing the neuroinflammatory response at 6 months post TBI using OX-6 antibody against MHCII-expressing cells (Raivich et al., 1999; O'Keefe et al., 2002). Neuroinflammatory processes, characterized by activated immune cells including microglia, dendritic cells, macrophages and monocytes, play crucial roles in the development and progression of neurodegenerative diseases such as dementia and the accumulation of senile plaques in AD, but the mechanism of action, especially for TBI, is yet to be elucidated (Povlishock and Cristman, 1995; Cho et al., 2011; Mizuno et al., 2011). Notwithstanding, the inflammatory response has both pro-inflammatory (or classical) response and anti-inflammatory (Th2/M2 or alternative) response. MHCII is a marker for inflammation, but it is not a specific marker for pro-inflammatory response because it is also expressed in anti-inflammatory cells (Marshall et al., 2013). Furthermore, T helper (Th) cells-mediated immune response requires the expression of MHCII in antigen presenting cells (microglia, macrophages, dendritic cells) to activate both M1/Th1 and M2/Th2 responses. Our present study implicates a potential pathological link between late stage TBI and AD as evidenced by activated neuroinflammatory cells and accumulation of APP+ in late stage TBI. Although traditionally shown to be expressed in neurons, APP+ cells are also detected in microglia and astrocytes (Haass et al., 1991). TBI as a risk factor for AD pathology may involve a dysfunctional immune clearance of APP+ and Aβ by activated MHCII+ cells and an aberrant overexpression of APP and Aβ (Selkoe, 1997; Sheng et al., 2003; Hickman et al., 2008). In support of the dysfunctional immune system hypothesis, deleting the TNFR1 in transgenic mice prevents learning and memory impairments (He et al., 2007). Additionally, injecting APPswe transgenic mice with lipopolysaccharide leads to an overexpression of APP and Aβ (Sheng et al., 2003). An aberrant overexpression of APP may precipitate during sub-acute stages and persists through late stage stages of TBI (Iwata et al., 2002; Uryu et al., 2007; Johnson et al., 2012; Mannix and Whalen, 2012).

We are cognizant that the present results are limited to a single time point whereby we evaluated neuroinflammation, altered neurogenesis and APP+ overexpression in an experimental model of late stage TBI. In addition, based on our present data, we recognize that our hypothesis warrants further investigations separate from the current study in order to further elucidate the mechanism of action by which inflammation influences the propagation and overexpression of APP in white and gray matter regions. Evaluation of the detrimental effect of secondary injuries across different time

points (i.e., acute, sub-acute, and delayed) coupled with anti-inflammatory treatments to assess the modulatory role of the immune system in neurogenesis and APP expression in TBI will further provide information about possible mechanisms. Another limitation of the study is that the model of TBI here is unilateral injury. Accordingly, the subsequent pathology arising from this unilateral injury, including the observed AD-like histological alteration (i.e., APP overexpression within the ipsilateral TBI hemisphere), cannot be claimed as a laterality event, but rather a consequence of the model. A series of studies is now underway to fully capture the MHCII and APP interaction after TBI, in particular detailing the progression of APP overexpression on proximal and remote white and gray matter regions and the delayed exacerbation of MCHII inflammatory cells in specific brain regions displaying APP overexpression.

As seen in this study, exacerbation of activated immune cells was detected not only on ipsilateral to injury but also throughout the brain after 6 months from the initial injury. Treatments targeting the secondary cell death characterized by neuroinflammation post TBI have been proposed to manage the multifactorial nature of the disease progression after TBI (Tajiri et al., 2013; Acosta et al., 2014; Lozano et al., 2015). For instance, we have previously shown that combined therapy of human umbilical cord blood cells (hUCB) and granulocyte colony stimulation factor (G-CSF) optimally abrogated exacerbation of active inflammatory cells rescuing neurogenesis and ameliorating motor function deterioration in chronic TBI animals (Acosta et al., 2014). In addition, we have reported that selective inhibitors of nuclear export (SINE) sequestered TBI-induced neuroinflammation-related proteins (i.e., NF-(k)B, AKT, FOXP1), and it decreased TBI-induced cell death in the core impact area and improved motor and neurological outcomes (Tajiri et al., 2013). Interestingly, in relation to APP and inflammation, it has been shown that hyperactivity of GSK-3, a promoter of inflammation, causes dysregulation on the APP cleavage and instigates its abnormal accumulation. Lithium, a GSK-3 inhibitor have been shown to have anti-amyloid properties and to have neuroprotective effects on hippocampal tissue (Phiel et al., 2003). In addition, Curcumin, the spice from turmeric and curry has been shown to be highly antioxidant and anti-inflammatory and decrease the Aβ levels and plaque load in aged transgenic APP mice (tg2576) (Lim et al., 2001). Accordingly, an anti-inflammatory therapy could be a promising treatment to decrease inflammation and APP in diseases whereby primary and secondary damage are followed by neuroinflammatory responses. Previous studies have also demonstrated that attenuation of microglial activation after TBI is associated with decreases on Aβ precursor and amelioration of behavioral outcome after TBI. Minocycline, simvastatin, a 3-hydroxy-3-methylglutaryl coenzyme A reductase inhibitors (statins) have all been shown to have anti-inflammatory effects, to mitigate increases in Aβ and to ameliorate TBI-induce behavioral deficits (Abrahamson et al., 2009; Homsi et al., 2010). These studies support our hypothesis that manipulating the inflammatory response after TBI might reduce APP overexpression and other AD-like pathologic markers.

The present study highlights the pivotal role of APP in chronic neuroinflammation, in that the same brain regions with exacerbated inflammatory cells displayed aberrant APP accumulation, altogether suggesting a close pathological interaction between TBI and AD, at least in the long-term inflammatory response associated with the disease progression. Recognizing that APP closely accompanies late stage TBI suggests that treatments designed to target unloading aberrant APP accumulation may be therapeutic for TBI.

Authors' Contributions

S.A.A. and C.V.B. conceived the study, participated in its coordination, and wrote the manuscript. S.A.A., C.V.B., Y.K., and N.T. performed the experiments and analyzed the data. All authors read and approved the final manuscript.

Acknowledgment

This work was supported by U.S. Department of Defense, W81XWH-11-1-0634.

Literature Cited

Abrahamson EE, Ikonomovic MD, Edward Dixon C, DeKosky ST. 2009. Simvastatin therapy prevents brain trauma-induced increases in β-amyloid peptide levels. Ann Neurol 66:407–414.
Acosta SA, Tajiri N, Shinozuka K, Ishikawa H, Grimmig B, David Diamond, Sanberg PR, Bickford PC, Kaneko Y, Borlongan CV. 2013. Long-term upregulation of inflammation and suppression of cell proliferation in the brain of adult rats exposed to traumatic brain injury using the controlled cortical impact model. PLoS ONE 8:e53376.
Acosta SA, Tajiri N, Shinozuka K, Ishikawa H, Sanberg PR, Sanchez-Ramos J, Song S, Kaneko Y, Borlongan CV. 2014. Combination therapy of human umbilical cord blood cells and granulocyte colony stimulating factor reduces histopathological and motor impairments in an experimental model of chronic traumatic brain injury. PLoS ONE 9:e90953.
Amaral DG, Witter MP. 1989. The three-dimensional organization of the hippocampal formation: A review of anatomical data. Neuroscience 31:571–591.
Aungst SL, Kabadi SV, Thompson SM, Stoica BA, Faden AI. 2014. Repeated mild traumatic brain injury causes chronic neuroinflammation, changes in hippocampal synaptic plasticity, and associated cognitive deficits. J Cereb Blood Flow Metab 34:1223–1232.
Blumbergs PC, Scott G, Manavis J, Wainwright H, Simpson DA, McLean AJ. 1994. Staining of amyloid precursor protein to study axonal damage in mild head injury. Lancet 344:1055–1056.
Borgens RB, Liu-Snyder P. 2012. Understanding secondary injury. Q Rev Biol 87:89–127.
Chauhan NB. 2014. Chronic neurodegenerative consequences of traumatic brain injury. Restor Neurol Neurosci 32:337–365.
Chen Y, Liu W, McPhie DL, Hassinger L, Neve R. 2003. APP-BP1 mediates APP-induced apoptosis and DNA synthesis and is increased in Alzheimer's disease brain. J Cell Biol 163:27–33.
Cho SH, Sun B, Zhou Y, Kauppinen TM, Halabisky B, Wes P, Ransohoff RM, Gan L. 2011. CX3CR1 protein signaling modulates microglial activation and protects against plaque-independent cognitive deficits in a mouse model of Alzheimer disease. J Biol Chem 286:32713–32722.
Dixon CE, Kochanek PM, Yan HQ, Schiding JK, Griffith RG, Baum E, Marion DW, DeKosky ST. 1999. One-year study of spatial memory performance, brain morphology, and cholinergic markers after moderate controlled cortical impact in rats. J Neurotrauma 16:109–122.
Elder GA. 2012. Blast exposure induces post-traumatic stress disorder-related traits in a rat model of mild traumatic brain injury. J Neurotrauma 29:2564–2575.
Fabrizio KS, Keltner NL. 2010. Traumatic brain injury in operation enduring freedom/operation iraqi freedom: A primer. Nurs Clin North Am 45:569–580.
Faul M, Xu L, Walt M, Coronado V. 2010. Traumatic brain injury in the United States: Emergency department visits, hospitalizations, and deaths, 2002–2006. Atlanta, GA: Centers for Disease Control and Prevention, National Center for Injury Prevention and Control.
Fleminger S, Oliver DL, Lovestone S, Rabe-Hesketh S, Giora A. 2003. Head injury as a risk factor for Alzheimer's disease: The evidence 10 years on; a partial replication. J Neurol Neurosurg Psychiatry 74:857–862.
Gardner RC, Yaffe K. 2015. Epidemiology of mild traumatic brain injury and neurodegenerative disease. Mol Cell Neurosci 66:75–80.
Ge Y, Patel MB, Chen Q, Grossman EJ, Zhang K, Miles L, Babb JS, Reaume J, Grossman RI. 2009. Assessment of thalamic perfusion in patients with mild traumatic brain injury by true FISP arterial spin labelling MR imaging at 3T. Brain Inj 23:666–674.
Ghajar J. 2000. Traumatic brain injury. Lancet 356:923–929.
Glover LE, Tajiri N, Lau T, Kaneko Y, van Loveren H, Borlongan CV. 2012. Immediate, but not delayed, microsurgical skull reconstruction exacerbates brain damage in experimental traumatic brain injury model. PLoS ONE 7:e33646.
Gottlieb S. 2000. Head injury doubles the risk of Alzheimer's disease. BMJ 321:1100.
Hayward NM, Tuunanen PI, Immonen R, Ndode-Ekane XE, Pitkänen A, Gröhn O. 2011. Magnetic resonance imaging of regional hemodynamic and cerebrovascular recovery after lateral fluid-percussion brain injury in rats. J Cereb Blood Flow Metab 31:166–177.
Hayward NM, Immonen R, Tuunanen PI, Ndode-Ekane XE, Gröhn O, Pitkänen A. 2010. Association of chronic vascular changes with functional outcome after traumatic brain injury in rats. J Neurotrauma 27:2203–2219.
Haass C, Hung Y, Selkoe DJ. 1991. Processing of, β-amyloid precursor protein in microglia and astrocytes favors an internal localization over constitutive secretion. J Neurosci 11:3783–3793.
He P, Zhong Z, Lindholm K, Berning L, Lee W, Lemere C, Staufenbiel M, Li R, Shen Y. 2007. Deletion of tumor necrosis factor death receptor inhibits amyloid beta generation and prevents learning and memory deficits in Alzheimer's mice. J Cell Biol 178:829–841.
Hernandez-Ontiveros DG, Tajiri N, Acosta S, Giunta B, Tan J, Borlongan CV. 2013. Microglia activation as a biomarker for traumatic brain injury. Front Neurol 4:30.
Homsi S, Piaggio T, Croci N, Noble F, Plotkine M, Marchand-Leroux C, Jafarian-Tehrani M. 2010. Blockade of acute microglial activation by minocycline promotes neuroprotection and reduces locomotor hyperactivity after closed head injury in mice: A twelve-week follow-up study. J Neurotrauma 27:911–921.
Hong YT, Veenith T, Dewar D, Outtrim JG, Mani V, Williams C, Pimlott S, Hutchinson PJ, Tavares A, Canales R, Mathis CA, Klunk WE, Aigbirhio FI, Coles JP, Baron JC, Pickard JD, Fryer TD, Stewart W, Menon DK. 2014. Amyloid imaging with carbon 11—Labeled pittsburgh compound B for traumatic brain injury. JAMA Neurol 71:23–31.
Hickman SE, Allison EK, EL Khoury J. 2008. Microglial dysfunction and defective β-amyloid clearance pathways in aging Alzheimer's disease mice. J Neurosci 28:8354–8360.

Hortobágyi T, Wise S, Hunt N, Cary N, Djurovic V, Fegan-Earl A, Shorrock K, Rouse D, Al-Sarraj S. 2007. Traumatic axonal damage in the brain can be detected using b-APP immunohistochemistry within 35min after head injury to human adults. Neuropathol Appl Neurobiol 33:226–237.
Iwata A, Chen XH, McIntosh TK, Browne KD, Smith DH. 2002. Long-term accumulation of amyloid-beta in axons following brain trauma without persistent upregulation of amyloid precursor protein genes. J Neuropathol Exp Neurol 61:1056–1068.
Johnson VE, Stewart JE, Begbie FD, Trojanowski JQ, Smith DH, Stewart W. 2013. Inflammation and white matter degeneration persist for years after a single traumatic brain injury. Brain 136:28–42.
Johnson VE, Stewart W, Smith DH. 2012. Widespread tau and amyloid-beta pathology many years after a single traumatic brain injury in humans. Brain Pathol 22:142–149.
Kempermann G. 2002. Why new neurons? Possible functions for adult hippocampal neurogenesis. J Neurosci 22:635–638.
Little DM, Kraus MF, Joseph J, Geary EK, Susmaras T, Zhou XJ, Pliskin N, Gorelick PB. 2010. Thalamic integrity underlies executive dysfunction in traumatic brain injury. Neurology 74:558–564.
Lim GP, Chu T, Yang F, Beech W, Frautschy SA, Cole GM. 2001. The curry spice curcumin reduces oxidative damage and amyloid pathology in an alzheimer transgenic mouse. J Neurosci 21:8370–8377.
Loane DJ, Byrnes KR. 2010. Role of microglia in neurotrauma. Neurotherapeutics 7:366–377.
Lozano D, Gonzales-Portillo GS, Acosta S, de la Pena I, Tajiri N, Kaneko Y, Borlongan CV. 2015. Neuroinflammatory responses to traumatic brain injury: Etiology, clinical consequences, and therapeutic opportunities. Neuropsychiatr Dis Treat 11:97–06.
Mannix RC, Whalen MJ. 2012. Traumatic brain injury, microglia, and Beta amyloid. Int J Alzheimers Dis 2012:608732.
Marshall SA, McClain JA, Kelso ML, Hopkins DM, Pauly JR, Nixon K. 2013. Microglial activation is not equivalent to neuroinflammation in alcohol-induced neurodegeneration: The importance of microglia phenotype. Neurobiol Dis 54:239–251.
Mayhew TM. 1991. The new stereological methods for interpreting functional morphology from slices of cells and organs. Exp Physiol 76:639–665.
McLaurin J, Almazan G, Williams K, Antel JP. 1995. Immortalization and characterization of rat microglial cells. Neuropathol Appl Neurobiol 21:302–311.
Mizuno T, Doi Y, Mizoguchi H, Jin S, Noda M, Sonobe Y, Takeuchi H, Suzumura A. 2011. Interleukin-34 selectively enhances the neuroprotective effects of microglia to attenuate oligomeric amyloid-β neurotoxicity. Am J Pathol 179:2016–2027.
Murakami N, Yamaki T, Iwamoto Y, Sakakibara T, Kobori N, Fushiki S, Ueda S. 1998. Experimental brain injury induces expression of amyloid precursor protein, which may be related to neuronal loss in the hippocampus. J Neurotrauma 15:993–903.
Nakashiba T, Young JZ, McHugh TJ, Buhl DL, Tonegawa S. 2008. Transgenic inhibition of synaptictransmission reveals role of CA3 output in hippocampal learning. Science 319:1260–1264.
O'Keefe GM, Nguyen VT, Benveniste EN. 2002. Regulation and function of class II major histocompatibility complex, CD40, and B7 expression in macrophages and microglia: Implications in neurological diseases. J Neurovirol 8:496–512.
Park MS, Oh HA, Ko IG, Kim SE, Kim SH, Kim CJ, Kim HB, Kim H. 2014. Influence of mild traumatic brain injury during pediatric stage on short-term memory and hippocampal apoptosis in adult rats. J Exerc Rehabil 10:148–154.
Paxinos G, Watson C. 2005. The rat brain in stereotaxic coordinates. San Diego, CA: Academic Press.
Phiel CJ, Wilson CA, Lee VM, Klein PS. 2003. GSK-3alpha regulates production of Alzheimer's disease amyloid-beta peptides. Nature 423:435–439.
Povlishock JT, Cristman CW. 1995. The pathobiology of traumatically induced axonal injury in animals and human: A review of current thoughts. J Neurotrauma 12:555–564.
Raivich G, Bohatschek M, Kloss CU, Werner A, Jones LL, Kreutzberg GW. 1999. Neuroglial activation repertoire in the injured brain: Graded response, molecular mechanisms and cues to physiological function. Brain Res Brain Res Rev 30:77–105.
Ramlackhansingh AF, Brooks DJ, Greenwood RJ, Bose SK, Turkheimer FE, Kinnunen KM, Gentleman S, Heckemann RA, Gunanayagam K, Gelosa G, Sharp DJ. 2011. Inflammation after trauma: Microglial activation and traumatic brain injury. Ann Neurol 70:374–383.
Reddy PH, Manczak M, Mao P, Calkins MJ, Reddy AP, Shirendeb U. 2010. Amyloid-beta and mitochondria in aging and Alzheimer's disease: Implications for synaptic damage and cognitive decline. J Alzheimers Dis 20:S499–S512.
Rogers JM, Read CA. 2007. Psychiatric comorbidity following traumatic brain injury. Brain Inj 21:1321–1333.
Rola R, Mizumatsu S, Otsuka S, Morhardt DR, Noble-Haeusslein LJ, Fishman K, Potts MB, Fike JR. 2006. Alterations in hippocampal neurogenesis following traumatic brain injury in mice. Exp Neurol 202:189–199.
Schiff ND. 2010. Recovery of consciousness after brain injury: A mesocircuit hypothesis. Trends Neurosci 33:1–9.
Schmidt OI, Heyde CE, Ertel W, Stahel PF. 2005. Closed head injury—An inflammatory disease? Brain Res Brain Res Rev 48:388–99.
Scholzen T, Gerdes J. 2000. The Ki-67 protein: From the known and the unknown. J Cell Physiol 182:311–322.
Scoville WG. 1954. The limbic lobe in man. J Neurosurg 11:64.
Selkoe DJ. 1997. Alzheimer's disease: Genotypes, phenotypes, and treatments. Science 275:630–631.
Sharp DJ, Scott G, Leech R. 2014. Network dysfunction after traumatic brain injury. Nat Rev Neurol 10:156–166.
Sheng JG, Bora SH, Xu G, Borchelt DR, Price DL, Koliatsos VE. 2003. Lipopolysaccharide-induced-neuroinflammation increases intracellular accumulation of amyloid precursor protein and amyloid beta peptide in APPswe transgenic mice. Neurobiol Dis 14:133–45.
Soldatovic-Stajic B, Misic-Pavkov G, Bozic K, Novovic Z, Gajic Z. 2014. Neuropsychological and neurophysiological evaluation of cognitive deficits related to the severity of traumatic brain injury. Eur Rev Med Pharmacol Sci 18:1632–1637.
Strittmatter WJ, Roses AD. 1995. Apolipoprotein E and Alzheimer disease. PNAS 92911:4725.
Tajiri N, Kellogg SL, Shimizu T, Arendash GW, Borlongan CV. 2013. Traumatic brain injury precipitates cognitive impairment and extracellular Aβ aggregation in Alzheimer's disease transgenic mice. PLoS ONE 8:e8851.
Thurman DJ, Alverson C, Dunn KA, Guerrero J, Sniezek JE. 1999. Traumatic brain injury in the United States: A public health perspective. J Head Trauma Rehabil 14:602–615.
Uryu K, Chen XH, Martinez D, Browne KD, Johnson VE, Graham DI, Lee VM, Trojanowski JQ, Smith DH I. 2007. Multiple proteins implicated in neurodegenerative diseases accumulate in axons after brain trauma in humans. Exp Neurol 208:185–192.
Vasterling JJ, Brailey K, Proctor SP, Kane R, Heeren T, Franz M. 2012. Neuropsychological outcomes of mild traumatic brain injury, post-traumatic stress disorder and depression in Iraq-deployed US Army soldiers. Br J Psychiatry 201:186–192.
Wang GH, Jiang ZL, Li YC, Li X, Shi H, Gao YQ, Vosler PS, Chen J. 2011. Free-radical scavenger edaravone treatment confers neuroprotection against traumatic brain injury in rats. J Neurotrauma 28:2123–2134.
Wang G, Jiang X, Pu H, Zhang W, An C, Hu X, Liou AK, Leak RK, Gao Y, Chen J. 2013. Scriptaid, a novel histone deacetylase inhibitor, protects against traumatic brain injury via modulation of PTEN and AKT pathway: Scriptaid protects against TBI via AKT. Neurotherapeutics 10:124–142.
Werner C, Engelhard K. 2007. Pathophysiology of traumatic brain injury. Br J Anaesth 99:4–9.
Zhao J, O'Connor T, Vassar R. 2011. The contribution of activated astrocytes to Abeta production: Implications for Alzheimer's disease pathogenesis. J Neuroinflammation 8:150.